Electron Affinities of C_{60} and C_{70} and Cooling of Their Anions

J. E. Navarro Navarrete,[1] P. Martini,[1] S. Rosén,[1] A. Simonsson,[1] P. Reinhed,[1] M. Björkhage,[1] M. Blom,[1] J. Alexander,[1] M. C. Ji,[1] M. K. Kristiansson,[1] R. Barzaga,[2] F. Aguilar-Galindo,[3,4] M. Alcamí,[3,4,5] S. Diaz-Tendero,[3,4,6] K. Hansen,[7] M. Gatchell,[1] H. Cederquist,[1] H. T. Schmidt,[1] and H. Zettergren[1,*]

[1]*Department of Physics, Stockholm University, AlbaNova, Stockholm SE-106 91, Sweden*
[2]*Departamento de Física and IUdEA, Universidad de La Laguna, 38200 Tenerife, Spain*
[3]*Departamento de Química, Universidad Autónoma de Madrid, 28049 Madrid, Spain*
[4]*Institute for Advanced Research in Chemistry (IAdChem), Universidad Autónoma de Madrid, 28049 Madrid, Spain*
[5]*Instituto Madrileño de Estudios Avanzados en Nanociencia (IMDEA-Nano), Campus de Cantoblanco, 28049 Madrid, Spain*
[6]*Condensed Matter Physics Center (IFIMAC), Universidad Autónoma de Madrid, 28049 Madrid, Spain*
[7]*Center for Joint Quantum Studies, Department of Physics, School of Science, Tianjin University, 92 Weijin Road, Tianjin 300072, China*

(Received 29 January 2025; accepted 16 October 2025; published 20 November 2025)

We combine cryogenic storage of fullerene anions up to minutes with laser photo-detachment spectroscopy and measure the electron affinities to be 2.684(3) eV for C_{60} and 2.7665(3) eV for C_{70}, which settle long-standing issues concerning these values. We find that C_{70}^- cools more efficiently than C_{60}^- and that this is due to differences in photon emission from electronically excited states populated by inverse internal conversion (recurrent fluorescence). We also find that intramolecular vibrational redistribution is no longer effective at low internal energies of C_{60}^- or C_{70}^-. Radiative cooling becomes extremely slow below intramolecular vibrational redistribution decoupling energies of 0.32(2) and 0.13(3) eV for C_{60}^- and C_{70}^-, respectively.

DOI: 10.1103/j2sv-7v9l

When isolated polyatomic molecules are excited in interactions with energetic particles or photons, the excess energy is often rapidly redistributed across all internal degrees of freedom. This may then lead to molecular fragmentation, electron emission, isomerization, or radiative cooling, or to combinations of such processes in different sequences on timescales ranging from picoseconds to minutes and beyond [1]. A detailed knowledge of this dynamics is key to advance the understanding of the destruction and survival of molecules in extraterrestrial environments, such as the interstellar medium, where more than 300 molecular species have been identified as neutrals, cations, or anions [2,3]. These systems range in complexity from simple diatomics [4] to chain- [5] and ring-formed molecules [6,7] to polycyclic aromatic hydrocarbons [8,9] and fullerenes (C_{60} and C_{70}) [10–14]. The ionic forms are of particular interest as they may play key roles for the chemical evolution through barrierless reactions with neutrals or counterions [15]. Additionally, the ion population is an indicator for the local astrophysical conditions and in particular of particle densities and the properties of the radiation fields [16].

Molecular properties such as high electron affinities, large heat capacities, and fast radiative cooling increase the probability that an excited anionic molecular system will stay intact on long timescales. Fullerene anions have all these characteristics and are thus likely to be omnipresent in space [13,17]. Pioneering room-temperature storage-ring experiments have revealed that complex molecular ions cool efficiently and survive even when their internal energies are well above the dissociation energy thresholds, which for fullerenes are around 10 eV [18,19]. For fullerenes, the cooling may be described by a statistical model developed in Ref. [20] where recurrent fluorescence emission of photons is assumed to be driven by a broad surface plasmon resonance. The absolute radiative cooling rates of C_{60}^- have been measured before for internal energies in the range 9.7–14.1 eV by combining ion-beam storage with laser photo-detachment techniques [21,22]. The corresponding results are in good agreement with those from a statistical model using the electron affinity (EA) of C_{60} as the activation energy in the rate equation for electron emission [21]. High-precision laser photo-electron spectroscopy (LPES) measurements reported EAs for C_{60} and C_{70} to be 2.6835(6) [23] and 2.765(10) eV [24], respectively. On the other hand, laser photo-detachment threshold spectroscopy (LPTS) studies reported systematically lower values of 2.664(5) [25] and 2.666(1) eV [26] for C_{60} and

*Contact author: henning@fysik.su.se

2.676(1) eV for C_{70} [26]. The discrepancy of 18 standard deviations for the EA of C_{60} has been suggested to be caused by calibration issues in the LPES studies [23] and/or vibrational hot band contributions in the LPTS measurements [25].

In this Letter, we settle the long-standing issue on the EA values and provide unprecedented details on the cooling dynamics of C_{60}^- and C_{70}^- in new time domains. We combine cryogenically cooled ion-beam storage [27,28] with LPTS measurements and radiative cooling models using results from our high-level *ab initio* multiconfigurational calculations of excited states in C_{60}^- and C_{70}^-. We confirm that internally hot C_{70}^- cools more rapidly than C_{60}^- [29] and show that this is due to recurrent fluorescence via a low-lying electronically excited state. On longer timescales exceeding hundreds of milliseconds, IR emission due to vibrational transitions is the dominant cooling mechanism. Here, we determine its effectiveness by monitoring the vibrational hot band contributions to the electron detachment signal during ion storage of up to 100 s. We find that IR emission is strongly quenched after a few seconds of storage as the internal energies then have become too low for intramolecular vibrational redistribution (IVR) to be effective, thus preventing efficient energy flow between vibrational modes. We find that this decoupling, defined in Ref. [30], occurs for internal energies below 0.32(2) and 0.13(3) eV for C_{60}^- and C_{70}^-, respectively.

The experiments were carried out at the DESIREE (Double ElectroStatic Ion-Ring ExpEriment) facility [31,32] at Stockholm University. Rovibrationally excited fullerene anions (C_{60}^- and C_{70}^-) were produced using an electron attachment ion source based on the design by Yamada *et al.* [33]. The anions were accelerated to 25 keV (C_{60}^-) and 20 keV (C_{70}^-) in separate experiments; mass to charge was selected by means of a 90° bending magnet and transported over 11 m to one of the DESIREE storage rings as indicated in Fig. 1. The ion beams were chopped into pulses to match the revolution times of 108 and 130 μs for C_{60}^- and C_{70}^-, respectively.

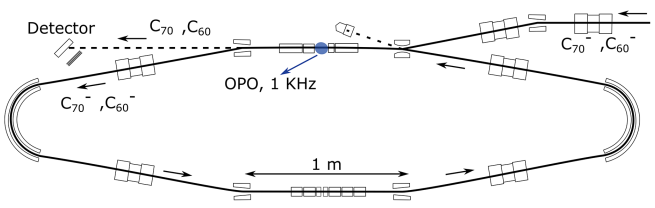

FIG. 1. Schematic of the experimental setup used to study spontaneous decays of internally hot fullerene anions and for laser photo-detachment spectroscopy of the anions as they cool in the cryogenic environment (13 K) at a residual gas pressure lower than 10^{-14} mbar [31,32]. The excellent vacuum conditions allow studies on timescales exceeding minutes. The optical parametric oscillator (OPO) laser pulse is crossed perpendicularly with the stored ion beam.

We first studied spontaneous electron emission, $C_{60/70}^- \rightarrow C_{60/70} + e^-$, from the fullerene anions that were cold enough to survive the transport to the ring but still sufficiently hot to emit electrons during storage. We recorded the yields of neutralized C_{60}^- and C_{70}^- separately as functions of storage time using the detector facing the upper straight section in Fig. 1. The C_{60}^- and C_{70}^- neutralization signals (after background subtraction) are shown in the upper and bottom left panels of Fig. 2, respectively (note the log-log scales). The decay curves are well-reproduced by power laws that are exponentially quenched at a characteristic time (τ), $R(t) \propto t^p e^{-t/\tau}$, which are indicative of the evolution of broad internal energy distributions of the ensembles of stored ions [34,35]. From a fit (solid black line in Fig. 2) to the experimental data, we find that $\tau = 10.7$ ms for C_{60}^-, which is somewhat larger than the values reported in Refs. [18,21,22]. However, different definitions of the characteristic time were used in those studies [18,21,22], where the internal energy distributions may also have differed somewhat from the present

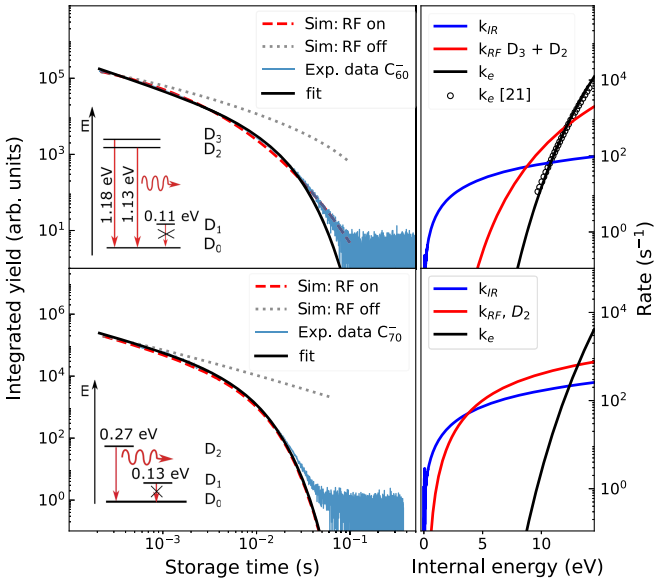

FIG. 2. Left panels: spontaneous decay measurements (blue lines) for C_{60}^- (top) and C_{70}^- (bottom). The black curves are fits with the formula $R(t) = t^p e^{-t/\tau}$ yielding $p = -0.811(1)$ and $\tau = 10.74(2)$ ms for C_{60}^-, and $p = -0.8239(7)$ and $\tau = 4.545(4)$ ms for C_{70}^-. The red curves are the simulations using Eq. (1) with the calculated rate constants shown in the right panels. The insets show schematic diagrams of the low-lying electronically excited states from the present *ab initio* calculations (see Appendix A and Supplemental Material [36]). The transitions that contribute to efficient cooling via recurrent fluorescence (RF) processes are indicated by arrows, while the arrows are crossed for those with very small or vanishing oscillator strengths. Right panels: calculated rate constants for the different decay processes, electron emission in black, RF in red, and IR emission in blue. The black open circles are the experimental results from Ref. [21].

one. Our fit for C_{70}^- yields $\tau = 4.5$ ms, which is clearly shorter than the corresponding result for C_{60}^-. Qualitatively, this difference is consistent with earlier results showing that C_{70}^- cools roughly a factor of 2 faster than C_{60}^- [29].

In order to gain further insight into the cooling dynamics, we calculate the rates for electron emission, recurrent fluorescence (RF), and vibrational deexcitations (IR emission) as functions of the internal ion energy, E. Here, the model key ingredients include the level densities for the initial and final states obtained from our density-functional theory calculations, and the frequency factors and activation energies for the different processes listed above taken from the literature and the present Letter (see Appendix A). The calculated rate constants for the three relaxation pathways—k_e for electron emission (solid black), k_{RF} for RF (red), and k_{IR} for IR emission (blue)—are shown in the top (C_{60}^-) and bottom (C_{70}^-) right panels of Fig. 2. The rate constant k_e for C_{60}^- is in close agreement with the results from Ref. [21], which are shown as black open circles (upper right panel) for internal energies in the 9–14 eV range. In this energy range, electron emission competes with both RF and IR emission, while the latter is dominating for lower internal energies of C_{60}^-. A similar overall trend is seen for C_{70}^- in the lower right panel of Fig. 2, albeit with a more significant RF rate at low internal energies.

We use our calculated rate constants to model the time dependence of the spontaneous electron emission rate [61],

$$R(t) \propto \int_0^\infty g(E,t) k_e(E) dE, \tag{1}$$

for an ensemble of stored anions with a normalized internal energy distribution, $g(E,t)$, that changes with the time, t, elapsed since the ions left the ion source. Here, $g(E, t = 0)$ is set to be a broad Boltzmann distribution ($T = 1300$ K) to reflect the ion source conditions. The radiative cooling rates (k_{RF} and k_{IR}) are affecting the time evolution of $g(E,t)$, via IVR [62,63], according to Eq. (A4) in Appendix A. The model decay curves for C_{60}^- and C_{70}^-, taking IR- and RF-decay processes into account, are shown as red dashed lines in the upper and lower left panels of Fig. 2, respectively. The results are in agreement with the experiments only when RF processes are included and we thus conclude that RF from low-lying electronically excited states with non-negligible oscillator strengths in our *ab initio* multiconfigurational calculations (see the insets in Fig. 2) are responsible for the efficient radiative cooling on these timescales. In the C_{70}^- case, the transition at 0.27 eV plays a key role and is the main reason why C_{70}^- cools much faster than C_{60}^-, while the RF rate for the lowest-lying electronically excited state in C_{70}^- at 0.13 eV is too low to have any significant influence on the cooling.

The background-subtracted data in Fig. 2 shows that the anions surviving > 100 ms are too cold to spontaneously emit electrons at a high rate. Thus, in order to monitor the radiative cooling dynamics occurring on longer timescales and to measure the fullerene electron affinities, we apply LPTS using a frequency doubled Nd:YAG Q-switch ns optical parametric oscillator laser system, with a repetition rate of 1 kHz. The laser beam crossed the anion beam at a right angle in one of the straight sections of the storage ring as shown in Fig. 1. The photo-detachment yield (neutral fullerenes) was then measured as a function of storage time using the same detector as in the spontaneous decay measurements (see Fig. 1). The photon energies were scanned across the detachment thresholds in variable steps, where the smallest steps were set at energies close to thresholds. The photon energy was changed after every injection cycle and this procedure was repeated a large number of times.

The photo-detachment threshold measurements for C_{60}^- and C_{70}^- are shown as black data points in the upper and lower panels of Fig. 3, respectively. These include all data recorded for ions stored up to 100 s. By performing a least-squares non-negative matrix factorization (NMF) analysis [64,65] (see Appendix B), we separate contributions from vibrational hot bands from contributions from internally cold molecules. The resulting spectra for the two contributions are shown as red and blue data points in Fig. 3 together with the reconstructed photo-detachment spectra (dashed light blue lines). We find that the contributions from the NMF components shown as red data points are decreasing with storage (cooling) time for both C_{60}^- and C_{70}^-, and these spectra are thus attributed to vibrational hot bands, while the NMF components shown as blue data points correspond to the spectra for internally cold molecules. Note that the thresholds for the individual rotational states are expected to be separated by very small amounts (μeV separations for nearby J states) and thus cannot be resolved in the present experiments. These behaviors are due to the rigid fullerene structures and hence the small differences in rotational constants as a function of rotational energy [66] and we have thus neglected such effects in the present analysis.

The insets in Fig. 3 are enlargements in the vicinities of the detachment thresholds for the cold component for each molecule. In order to determine the thresholds and hence EA values, we fit the results using the Wigner law,

$$\sigma(\epsilon) = (\epsilon - \mathrm{EA})^{L+1/2} \Theta(\epsilon - \mathrm{EA}), \tag{2}$$

where ϵ is the photon energy, L the angular momentum of the outgoing electron, and Θ a Heaviside step function accounting for the vanishing signal below threshold. For C_{60}^-, we follow Ref. [26] by setting $L = 0$ and using the threshold energy as a free parameter in the fit to the results, which yields a value of $\mathrm{EA}(C_{60}) = 2.684(3)$ eV. For C_{70}^-, we set the L value using a similar argument as Brink *et al.* [26] used for C_{60}^-. The extra electron in C_{70}^- occupies an

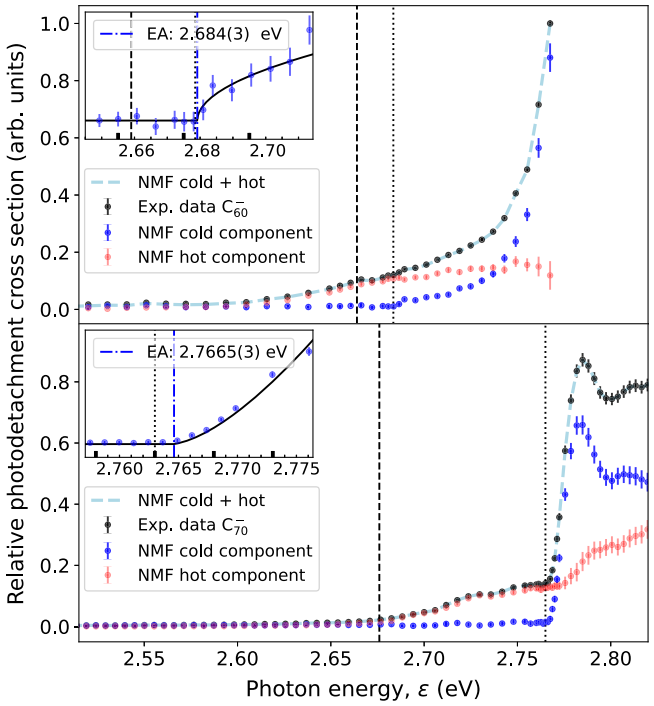

FIG. 3. Relative photo-detachment cross section as a function of photon energy (black data points) for C_{60}^- (upper panel) and C_{70}^- (lower panel). The blue and red points are the *cold* and *hot* components from the NMF analysis (see Appendix B), respectively, and the dashed light blue line is the sum of these two components. The insets show enlargements of the photo-detachment energy thresholds of the cold components. The electron affinities are determined to be 2.684(3) eV (C_{60}) and 2.7665(3) eV (C_{70}) from fits to the Wigner law [Eq. (2)] with $L = 0$ for C_{60}^- and $L = 1$ for C_{70}^- as indicated by black lines. Previous results from LPTS [26] and LPES [23,24] measurements are shown as dashed and dotted vertical lines, respectively.

orbital with e_1'' symmetry (D_{5h} point group) according to the calculations in Ref. [24]. This corresponds to $L = 2$ according to the character table for the D_{5h} point group, and the ejected electron must therefore have L values of 1 or 3. We find that our measurements are consistent with a p-wave threshold ($L = 1$), which gives $\mathrm{EA}(C_{70}) = 2.7665(3)$ eV from the Wigner law fit with the threshold energy as a free parameter.

The present EA values are indicated in the insets of Fig. 3 by the dot-dashed vertical lines, and the corresponding fits to the pure Wigner law [Eq. (2)] are shown as gray solid lines. These values are consistent with previous LPES measurements (dotted vertical lines in the insets and the main panels) reporting EAs for C_{60} and C_{70} to be 2.6835(6) [23] and 2.765(10) eV [24], respectively, but not with earlier LPTS results (dashed vertical lines) as these are systematically lower at 2.666(1) eV (C_{60}) [26] and 2.676 (1) eV (C_{70}) [26]. As the latter values fall in the regions of energies where we observe vibrational hot band contributions, we conclude that such contributions are likely the reason for the discrepancy between the LPES and earlier

TABLE I. Electron affinities (EAs) in eV from the present and earlier studies. The most precise experimental results are indicated in bold and are used to benchmark the present density-functional theory (DFT) results (see text).

	Present work		Earlier experimental work	
	LPTS	DFT	LPES	LPTS
C_{60}	2.684(3)	2.688	**2.6835(6)** [23]	2.666(1) [26]
C_{70}	**2.7665(3)**	2.712	2.765(10) [24]	2.676(1) [26]

LPTS values in the literature. We then use the present experimental result for C_{70} and the experimental result for C_{60} from Ref. [23] to benchmark density-functional theory calculations for reliable predictions of EAs for other fullerenes. Using a range of different functionals and basis sets (see Supplemental Material [36]) we find the overall best agreement with the BPW91 functional and the aug-cc-pVTZ basis set, yielding adiabatic EAs of 2.688 eV for C_{60} and 2.712 eV for C_{70}, respectively. These results are shown in Table 1 together with the present and earlier experimental results, where the recommended (most precise) values are shown in bold.

The time-dependent vibrational hot band contributions provide information on the ultraslow cooling dynamics. This is illustrated in Fig. 4 where we show the integrated intensity for photon energies (ϵ) ranging from 2.53 eV up to the EA value (open black circles) as a function of storage time for C_{60}^- (upper left panel) and C_{70}^- (lower left panel). The experimental results display a similar behavior for the two fullerenes and follow the mean value of the internal energy distribution (red dashed lines) from the present statistical model calculations (see Appendix A) up to a few seconds. The changes in these mean values reflect how the internal energy distributions shown in the right panels of Fig. 4 are evolving in time due to radiative cooling via IR emission, which dominates at low internal energies (see the right panels in Fig. 2). However, on still longer timescales, and hence for even lower internal energies, the experimental results show that the anions cool much less efficiently via IR emission than predicted by the present model where IVR is assumed to be effective for all excitation energies, E. This suggests that it is not possible for the internal energy to flow efficiently from IR-inactive to IR-active modes at sufficiently low values of E. To account for such an effect in our simulations, we follow a similar procedure as in Ref. [62] for the time evolution of the internal energy distribution when $E < E_{\mathrm{DEC}}$,

$$g(E, t+dt) = \frac{1}{N}\sum_{s=1}^{N} g(E,t)e^{-k_{\mathrm{IR}_s}(E)dt} + \frac{1}{N}\sum_{s=1}^{N} g(E+h\nu_s, t)(1-e^{-k_{\mathrm{IR}_s}(E+h\nu_s)dt}), \tag{3}$$

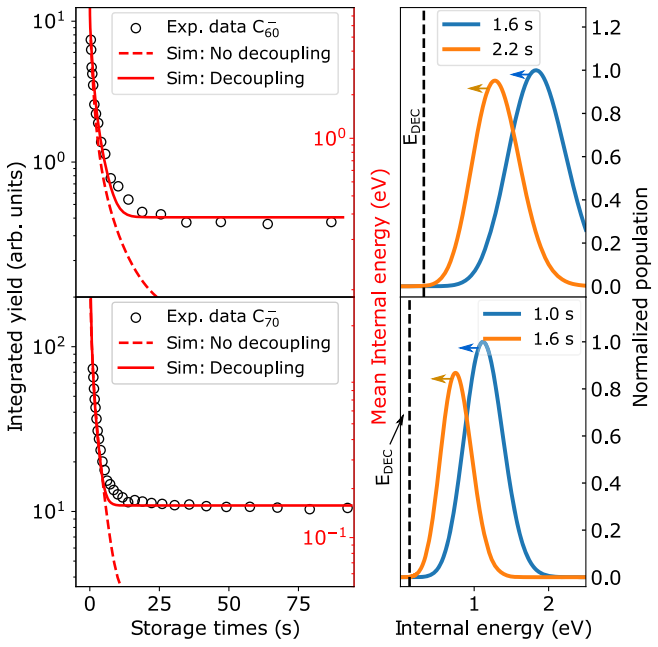

FIG. 4. Left panels: integrated counts of the photo-detachment spectra below the detachment (EA) threshold (open circles referring to the left vertical axes) as a function of storage time for C_{60}^- (upper panel) and C_{70}^- (lower panel). The red dashed curves (referring to the right vertical axes) are the mean internal energies $[\int_0^\infty Eg(E,t)dE]$ from the present simulations of the cooling dynamics assuming IVR to be valid at all times. The red solid curves (right vertical axes) are the corresponding results when IVR is only possible for internal energies exceeding the decoupling energies, E_{DEC} (see text). Right panels: snapshots of the simulated internal energy distributions as they approach (blue curves) and when their low energy tails (orange curves) reach $E_{\mathrm{DEC}}(C_{60}^-) = 0.32(2)$ eV and $E_{\mathrm{DEC}}(C_{70}^-) = 0.13(3)$ eV as shown as dashed vertical lines.

where the populations of the N individual vibrational modes are treated independently using a mean value approach. The resulting model decay curves are shown as solid red lines in the left panels of Fig. 4. These are from fits to the experimental data with the decoupling energy (E_{DEC}) as a free parameter, yielding $E_{\mathrm{DEC}}(C_{60}^-) = 0.32(2)$ and $E_{\mathrm{DEC}}(C_{70}^-) = 0.13(3)$ eV. These energies are similar to the decoupling energy reported for anthracene, $E_{\mathrm{DEC}}(C_{16}H_{10}) = 0.22$ eV, using picosecond time-resolved fluorescence spectroscopy [67]. In Fig. 4, we show that the model captures the main essence of the experimental results when decoupling is taken into account. This strongly quenches the cooling rates and hence the likelihood for internally hot fullerene anions to cool down to their vibrational ground states in isolation, e.g., in the interstellar medium.

In conclusion, by combining cryogenic ion-beam storage with laser photo-detachment techniques we settle the long-standing issues on the electron affinities of C_{60} and C_{70} and for C_{70} we present an experimental value that is about 30 times more precise than the earlier most precise result (see Table 1). We find that C_{70}^- cools more efficiently than C_{60}^- on timescales ranging from milliseconds to a few seconds, after which the cooling is strongly suppressed up to minutes and beyond for both anions. The latter reflects that IVR is no longer efficient for internal energies below the decoupling energies, which we here determine for fullerenes for the first time. These decoupling energies are measured to be $E_{\mathrm{DEC}}(C_{60}^-) = 0.32(2)$ and $E_{\mathrm{DEC}}(C_{70}^-) = 0.13(3)$ eV. The present combined experimental and theoretical approach may be readily used for studies of the cooling dynamics on extended timescales and for measurements of electron affinities and decoupling energies for molecular anions in general.

Acknowledgments—This work was performed at the Swedish National Infrastructure, DESIREE (Swedish Research Council Contracts No. 2017-00621, No. 2021-00155, and No. 2023-00170). H. Z., H. C., M. G., and H. T. S. thank the Swedish Research Council for individual project grants (with Contracts No. 2020-03437, No. 2023-03833, No. 2020-03104, and No. 2022-02822). Furthermore, H. C., H. T. S., H. Z., and M. G. acknowledge the project grant "Probing charge- and mass-transfer reactions on the atomic level" (No. 2018.0028) from the Knut and Alice Wallenberg Foundation. This publication is based upon work from COST Action CA18212—Molecular Dynamics in the GAS phase (MD-GAS), COST Action CA21126—Carbon molecular nanostructures in space (NanoSpace), and COST Action CA21101—Confined Molecular Systems: from the new generation of materials to the stars (COSY), supported by COST (European Cooperation in Science and Technology). We acknowledge the generous allocation of computer time at the Centro de Computación Científica at the Universidad Autónoma de Madrid (CCC-UAM). This work was partially supported by the MICINN—Spanish Ministry of Science and Innovation—Project No. PID2022-138470NB-I00, funded by MCIN/AEI/10.13039/501100011033, and the María de Maeztu Programme for Units of Excellence in R&D (CEX2023-001316-M). R. B. acknowledges the support from the State Research Agency (AEI) of the Ministry of Science, Innovation and Universities (MICIU) of the Government of Spain, and the European Regional Development Fund (ERDF), under Grants No. PID2020–115758 GB-I00/AEI/10.13039/501100011033 and PID2023-147325NB-I00/AEI/10.13039/501100011033.

Data availability—The data that support the findings of this article are openly available [68].

[1] H. Zettergren *et al.*, Eur. Phys. J. D **75**, 152 (2021).
[2] The Cologne Database for Molecular Spectroscopy, https://cdms.astro.uni-koeln.de/classic/molecules.
[3] B. A. McGuire, Astrophys. J. Suppl. Ser. **259**, 30 (2022).

[4] W. S. Adams, Astrophys. J. **93**, 11 (1941).
[5] W. W. Duley and A. Hu, Astrophys. J. **698**, 808 (2009).
[6] B. A. McGuire, A. M. Burkhardt, S. Kalenskii, C. N. Shingledecker, A. J. Remijan, E. Herbst, and M. C. McCarthy, Science **359**, 202 (2018).
[7] J. Cernicharo, A. M. Heras, A. G. G. M. Tielens, J. R. Pardo, F. Herpin, M. Guélin, and L. B. F. M. Waters, Astrophys. J. **546**, L123 (2001).
[8] A. M. Burkhardt, K. L. K. Lee, P. B. Changala, C. N. Shingledecker, I. R. Cooke, R. A. Loomis, H. Wei, S. B. Charnley, E. Herbst, M. C. McCarthy, and B. A. McGuire, Astrophys. J. Lett. **913**, L18 (2021).
[9] B. A. McGuire, R. A. Loomis, A. M. Burkhardt, K. L. K. Lee, C. N. Shingledecker, S. B. Charnley, I. R. Cooke, M. A. Cordiner, E. Herbst, S. Kalenskii, M. A. Siebert, E. R. Willis, C. Xue, A. J. Remijan, and M. C. McCarthy, Science **371**, 1265 (2021).
[10] J. Cami, J. Bernard-Salas, E. Peeters, and S. E. Malek, Science **329**, 1180 (2010).
[11] K. Sellgren, M. Werner, J. Ingalls, J. Smith, T. Carleton, and C. Joblin, Astrophys. J. Lett. **722**, L54 (2010).
[12] D. A. García-Hernández, A. Manchado, P. García-Lario, L. Stanghellini, E. Villaver, R. A. Shaw, R. Szczerba, and J. V. Perea-Calderón, Astrophys. J. Lett. **724**, L39 (2010).
[13] S. Iglesias-Groth, Mon. Not. R. Astron. Soc. **489**, 1509 (2019).
[14] E. Campbell, M. Holz, D. Gerlich, and J. Maier, Nature (London) **523**, 322 (2015).
[15] T. J. Millar, C. Walsh, and T. A. Field, Chem. Rev. **117**, 1765 (2017).
[16] A. G. G. M. Tielens, Rev. Mod. Phys. **85**, 1021 (2013).
[17] A. Sidhu, A. Tielens, E. Peeters, and J. Cami, Mon. Not. R. Astron. Soc. **522**, 3227 (2023).
[18] J. U. Andersen, C. Brink, P. Hvelplund, M. O. Larsson, B. Bech Nielsen, and H. Shen, Phys. Rev. Lett. **77**, 3991 (1996).
[19] J. U. Andersen, E. Bonderup, and K. Hansen, J. Chem. Phys. **114**, 6518 (2001).
[20] J. U. Andersen and E. Bonderup, Eur. Phys. J. D **11**, 413 (2000).
[21] K. Hansen, Phys. Rev. A **102**, 052823 (2020).
[22] A. E. K. Sundén, M. Goto, J. Matsumoto, H. Shiromaru, H. Tanuma, T. Azuma, J. U. Andersen, S. E. Canton, and K. Hansen, Phys. Rev. Lett. **103**, 143001 (2009).
[23] D.-L. Huang, P. D. Dau, H.-T. Liu, and L.-S. Wang, J. Chem. Phys. **140**, 224315 (2014).
[24] X.-B. Wang, H.-K. Woo, X. Huang, M. M. Kappes, and L.-S. Wang, Phys. Rev. Lett. **96**, 143002 (2006).
[25] K. Støchkel and J. U. Andersen, J. Chem. Phys. **139**, 164304 (2013).
[26] C. Brink, L. Andersen, P. Hvelplund, D. Mathur, and J. Voldstad, Chem. Phys. Lett. **233**, 52 (1995).
[27] H. T. Schmidt, G. Eklund, K. C. Chartkunchand, E. K. Anderson, M. Kamińska, N. de Ruette, R. D. Thomas, M. K. Kristiansson, M. Gatchell, P. Reinhed, S. Rosén, A. Simonsson, A. Källberg, P. Löfgren, S. Mannervik, H. Zettergren, and H. Cederquist, Phys. Rev. Lett. **119**, 073001 (2017).
[28] P. K. Najeeb, M. H. Stockett, E. K. Anderson, M. K. Kristiansson, P. Reinhed, A. Simonsson, S. Rosén, R. D. Thomas, K. C. Chartkunchand, H. Gnaser, R. Golser, D. Hanstorp, A. Larson, H. Cederquist, H. T. Schmidt, and H. Zettergren, Phys. Rev. Lett. **131**, 113003 (2023).
[29] J. U. Andersen, C. Gottrup, K. Hansen, P. Hvelplund, and M. O. Larsson, Eur. Phys. J. D **17**, 189 (2001).
[30] C. Joblin, D. Toublanc, D. P. Boissel, and A. G. G. M. Tielens, Mol. Phys. **100**, 3595 (2002).
[31] H. T. Schmidt *et al.*, Rev. Sci. Instrum. **84**, 055115 (2013).
[32] R. D. Thomas *et al.*, Rev. Sci. Instrum. **82**, 065112 (2011).
[33] K. Yamada, A. Chiba, Y. Hirano, and Y. Saitoh, AIP Conf. Proc. **2011**, 050020 (2018).
[34] J. U. Andersen, E. Bonderup, and K. Hansen, J. Phys. B **35**, R1 (2002).
[35] K. Hansen, Mass Spectrom. Rev. **40**, 725 (2021).
[36] See Supplemental Material at http://link.aps.org/supplemental/10.1103/j2sv-7v9l for the calculations of electron detachment energies and electronic excited states, which includes Refs. [37–60].
[37] A. D. Becke, J. Chem. Phys. **98**, 5648 (1993).
[38] C. Lee, W. Yang, and R. G. Parr, Phys. Rev. B **37**, 785 (1988).
[39] S. H. Vosko, L. Wilk, and M. Nusair, Can. J. Phys. **58**, 1200 (1980).
[40] P. J. Stephens, F. J. Devlin, C. F. Chabalowski, and M. J. Frisch, J. Phys. Chem. **98**, 11623 (1994).
[41] J.-D. Chai and M. Head-Gordon, Phys. Chem. Chem. Phys. **10**, 6615 (2008).
[42] A. D. Becke, Phys. Rev. A **38**, 3098 (1988).
[43] J. P. Perdew, *Electronic Structure of Solids '91*, edited by P. Ziesche and H. Eschrig (Akademie Verlag, Berlin, 1991), Chap. 11.
[44] J. P. Perdew, J. A. Chevary, S. H. Vosko, K. A. Jackson, M. R. Pederson, D. J. Singh, and C. Fiolhais, Phys. Rev. B **46**, 6671 (1992).
[45] J. P. Perdew, J. A. Chevary, S. H. Vosko, K. A. Jackson, M. R. Pederson, D. J. Singh, and C. Fiolhais, Phys. Rev. B **48**, 4978(E) (1993).
[46] J. P. Perdew, K. Burke, and Y. Wang, Phys. Rev. B **54**, 16533 (1996).
[47] W. J. Hehre, R. Ditchfield, and J. A. Pople, J. Chem. Phys. **56**, 2257 (1972).
[48] P. C. Hariharan and J. A. Pople, Theor. Chim. Acta **28**, 213 (1973).
[49] T. Clark, J. Chandrasekhar, G. W. Spitznagel, and P. V. R. Schleyer, J. Comput. Chem. **4**, 294 (1983).
[50] T. H. Dunning, J. Chem. Phys. **90**, 1007 (1989).
[51] R. A. Kendall, T. H. Dunning, and R. J. Harrison, J. Chem. Phys. **96**, 6796 (1992).
[52] M. J. Frisch *et al.*, Gaussian16 Revision C.01 (Gaussian Inc., Wallingford CT, 2016).
[53] D. Ampadu Boateng, G. L. Gutsev, P. Jena, and K. M. Tibbetts, J. Chem. Phys. **148**, 134305 (2018).
[54] D. Ampadu Boateng, M. D. Word, L. G. Gutsev, P. Jena, and K. M. Tibbetts, J. Phys. Chem. A **123**, 1140 (2019).
[55] G. L. Gutsev, H. A. López Peña, S. L. McPherson, D. A. Boateng, B. R. Ramachandran, L. G. Gutsev, and K. M. Tibbetts, J. Phys. Chem. A **124**, 3120 (2020).
[56] I. Fdez. Galván *et al.*, J. Chem. Theory Comput. **15**, 5925 (2019).
[57] J. Finley, P.-A. Malmqvist, B. O. Roos, and L. Serrano-Andrés, Chem. Phys. Lett. **288**, 299 (1998).
[58] J. Fulara, M. Jakobi, and J. P. Maier, Chem. Phys. Lett. **211**, 227 (1993).

[59] D. R. Lawson, D. L. Feldheim, C. A. Foss, P. K. Dorhout, C. M. Elliott, C. R. Martin, and B. Parkinson, J. Electrochem. Soc. **139**, L68 (1992).
[60] B. Kern, A. Böttcher, and D. Strelnikov, J. Phys. Chem. A **120**, 5868 (2016).
[61] J. Bernard, M. Ji, S. Indrajith, M. H. Stockett, J. E. Navarro Navarrete, N. Kono, H. Cederquist, S. Martin, H. T. Schmidt, and H. Zettergren, Phys. Chem. Chem. Phys. **25**, 10726 (2023).
[62] J. N. Bull, M. S. Scholz, E. Carrascosa, M. K. Kristiansson, G. Eklund, N. Punnakayathil, N. de Ruette, H. Zettergren, H. T. Schmidt, H. Cederquist, and M. H. Stockett, J. Chem. Phys. **151**, 114304 (2019).
[63] K. Hansen, O. Licht, A. Kurbanov, and Y. Toker, J. Phys. Chem. A **127**, 2889 (2023).
[64] D. D. Lee and H. S. Seung, Nature (London) **401**, 788 (1999).
[65] D. D. Lee and H. S. Seung, in *Advances in Neural Information Processing Systems 13: Proceedings of the 2000 Conference*, edited by T. Leen, T. Dietterich, and V. Tresp (Bradford Bks, 2001), p. 556.
[66] P. B. Changala, M. L. Weichman, K. F. Lee, M. E. Fermann, and J. Ye, Science **363**, 49 (2019).
[67] P. M. Felker and A. H. Zewail, Chem. Phys. Lett. **108**, 303 (1984).
[68] J. E. Navarro Navarrete *et al.*, "Dataset: Electron affinities of C_{60} and C_{70} and cooling of their anions", Zenodo 10.5281/zenodo.14760833 (2025).
[69] T. Beyer and D. F. Swinehart, Commun. ACM **16**, 379 (1973).
[70] D. V. Konarev, N. V. Drichko, and A. Graja, J. Chim. Phys. Phys.-Chim. Biol. **95**, 2143 (1998).
[71] K. Hansen, J. Andersen, H. Cederquist, C. Gottrup, P. Hvelplund, M. Larsson, V. Petrunin, and H. Schmidt, Eur. Phys. J. D **9**, 351 (1999).
[72] M. Kappe, P. Martini, A. Schiller, E. Gruber, F. Zappa, S. A. Krasnokutski, P. Scheier, and M. Gatchell, Phys. Rev. Res. **6**, L012045 (2024).
[73] M. H. Stockett, A. Subramani, C. Liu, S. J. P. Marlton, E. K. Ashworth, H. Cederquist, H. Zettergren, and J. N. Bull, J. Chem. Phys. **162**, 184306 (2025).

End Matter

Appendix A: Rate constants—We calculate the rate constant k_e for statistical electron emission using

$$k_e(E) = \nu_e \frac{\rho(E - EA)}{\rho(E)}, \tag{A1}$$

where ν_e is the frequency factor and EA is the electron affinities reported here: EA = 2.684(3) eV for C_{60} and EA = 2.7665(3) eV for C_{70}. We set $\nu_e = 3.5 \times 10^{13}$ s^{-1} for C_{60}^- following Ref. [21] and $\nu_e = 3 \times 10^{14}$ s^{-1} for C_{70}^-. Using these values in our master equation simulations described below, we reproduce the early (power-law) decays with initial internal energy distributions that are compatible with the ion source conditions in the two experiments (see the main text). The level densities for the initial, $\rho(E)$, and final, $\rho(E - EA)$, states in Eq. (A1) are computed using the Beyer-Swinehart algorithm [69] with vibrational frequencies from our density-functional theory calculations [B3LYP/6-31 + G(d) level of theory [37]].

We calculate the RF emission rate constant (k_{RF}) using

$$k_{RF}(E) = A_{r\to 0} \frac{\rho(E - h\nu_r)}{\rho(E)}, \tag{A2}$$

where $A_{r\to 0}$ is the Einstein coefficient connecting an electronically excited state $|r\rangle$ with excitation energy $h\nu_r$ and the electronic ground state $|0\rangle$. Here, we use results from our *ab initio* calculations of excited states and oscillator strengths, which were performed using multistate complete active space perturbation theory at second order (MS-CASPT2) and the cc-pVDZ basis set (see Ref. [36] for details. For C_{60}^-, we calculate $h\nu_r = 1.13$ eV and $h\nu_r = 1.18$ eV, which are in excellent agreement with the measured absorption band for the lowest energy dipole-allowed transitions from the electronic ground state [58,70–72]. For C_{70}^-, we find two low-lying electronically excited states ($h\nu_r = 0.13$ eV and $h\nu_r = 0.27$ eV) with nonzero oscillator strengths ($f > 10^{-5}$). Here, there are no measured values for comparisons as these electronic excitations are difficult to distinguish from vibrational excitations using IR spectroscopy. However, their existence has been inferred from comparisons between measured and calculated IR spectra [60].

We calculate the IR emission rate constant k_{IR} for vibrational deexcitations using the harmonic cascade approximation [62,63] for each individual vibrational mode s,

$$k_{IR_s}(E) = A_s \sum_{n=1}^{n \le E/h\nu_s} \frac{\rho(E - nh\nu_s)}{\rho(E)}, \tag{A3}$$

where A_s is the Einstein coefficient for the transition from the first excited vibrational state ($n = 1$) to the vibrational ground state ($n = 0$) of mode s. Note that the quanta (n) included in the energy-level-dependent oscillator strengths (nA_s) are absorbed in the expression for the density of states [see the supporting information in Ref. [63] for the derivation of Eq. (A3)]. In this model, only transitions where $\Delta n = -1$ are allowed [63]. Here, the vibrational frequencies and the Einstein coefficients are from our density-functional theory calculations and the level densities (ρ) from the same approach as for Eq. (A1) are used.

The rate constants are included in the master equation [73],

$$\frac{dg(E,t)}{dt} = -k_{tot}(E,t)g(E,t) + \sum_r k_{RF_r}(E + h\nu_r)g(E + h\nu_r) + \sum_s k_{IR_s}(E + h\nu_s)g(E + h\nu_s), \tag{A4}$$

which is used to describe the time evolution of the normalized internal energy distribution $g(E,t)$. The first term on the right-hand side in Eq. (A4) describes the decrease in the number of ions with the specific energy E at time t due to electron emission and radiative cooling, $k_{\mathrm{tot}} = k_{\mathrm{e}} + \sum_r k_{\mathrm{RF}_r} + \sum_s k_{\mathrm{IR}_s}$. The second and third terms in Eq. (A4) describe the increase in the number of ions with energy E at time t due to RF and IR emission from ions with internal energies $E + h\nu_r$ and $E + h\nu_s$, respectively.

Appendix B: Non-negative matrix factorization (NMF) analysis—Here, we set $\mathbf{X} \simeq \mathbf{WH}$, where $\mathbf{X}$ is an $n \times m$ matrix containing the experimental data and n and m are the number of time- and photon-energy bins, respectively. The NMF algorithm returns the weights $\mathbf{W} = n \times k$ and the components $\mathbf{H} = k \times m$ that minimize the Frobenius matrix norm $\|\mathbf{X} - \mathbf{WH}\|$ under the restriction that all elements in $\mathbf{H}$ and $\mathbf{W}$ are ≥ 0. We set the number of components, k, to 2 corresponding to one hot and one cold component (see the main text) and run the NMF algorithm a total of 2000 times with randomly generated $\mathbf{W}$ and $\mathbf{H}$ matrices where the experimental uncertainties are taken into account using the method described in Ref. [65]. These NMF spectra are averaged with the uncertainties in the individual data points set to their standard deviations.